Simulation and Modeling in Astrophysics
Project Report

Kostas Tsalapatas - s3479765
Erin Umuzigazuba - s3634701
Yiqi Wu - s3805352

December 22, 2023

Contents

1 Introduction

A generally accepted property of star clusters is that all stars within the cluster were formed around the same time from the same molecular cloud (MC). As a result, all stars should have approximately the same age and metallicity. This characteristic is true for young, open clusters, but not old, globular clusters. Multiple stellar populations with varying metallicities are observed in most globular clusters (GCs) in the Milky Way.

The nature of this unforeseen observation is thus far unknown. Numerous theories have been proposed. A well-liked theory disputes the assumption that all stars within a GC form simultaneously. Instead, it suggests that there are multiple epochs of star formation throughout a cluster's lifetime. To date, no conclusive evidence has been found proving any hypothesis (see [1, 2] for recent reviews).

For this project, we propose a new theory for the existence of multiple populations (MPs) in GCs. We believe that it is the result of the collision between a metal-poor GC and a metal-rich MC. As the GC passes through the MC, its stars accrete material from the cloud onto their surfaces. Seeing as we only observe the outer layer of a star, the stars that accreted mass appear to have a different, higher metallicity than the stars that did not accrete any material.

In this report, we demonstrate how we tested our hypothesis using the Astrophysical Multipurpose Software Environment (`AMUSE`)[1] [3, 4, 5, 6]. With this software, we simulated the collision between GCs and MCs. The model created for this purpose is implemented in the package `YESSIR`[2]. In Sec 2, observations of MPs in Galactic GCs, theories proposed to explain their existence and our hypothesis are discussed. In Sec 3, we describe the setup and implementation of our simulation. The results are given in Sec 4 and discussed in Sec 5. Lastly, in Sec 6, the conclusions of the project are presented.

2 Theory

2.1 Literature

In the present, open star clusters form when a MC becomes unstable, i.e. when it is no longer in hydrostatic equilibrium. MCs have approximately uniform densities on large scales. On smaller scales, however, the clouds consist of regions with various sizes and masses. These regions become unstable before the entire cloud and collapse into stars. Seeing as the metallicity is roughly the same throughout a MC, a group of stars with similar ages and chemical properties form [7].

Assuming that GCs similarly formed between 10 and 13 Gyr ago, their stars should also have similar ages and metallicities. However, when studying Galactic GCs, most clusters possess two types of stellar populations. The first population contains more evolved stars, all of which have a similar low metallicity. The second population is comprised of mostly main-sequence and giant stars with varying degrees of metal-rich chemical compositions.

[1] https://github.com/amusecode/amuse

[2] https://github.com/umuzigazuba/YESSIR

The existence of these distinct groups becomes noticeable when constructing a cluster's color-magnitude diagram (CMD) and drawing isochrones of stars with similar metallicities. An abundance of carbon, nitrogen and oxygen in a star makes it appear fainter in color than metal-poor stars. This is the result of an increased efficiency of the CNO-cycle. For the same reason, these stars have a lower effective temperature, making the presence of MPs also visible in Hertzsprung–Russell (HR) diagrams [8]. Consequently, the presence of MPs is visible in CMDs by the broadening and/or splitting of the main sequence and red-giant branches. Well-studied examples of this phenomenon in Galactic GCs are the broadened main sequence branch of 47 Tucanae, shown in the left plot of Fig 1, and the three main sequence branches of NGC 2808, shown in the right plot of Fig 1.

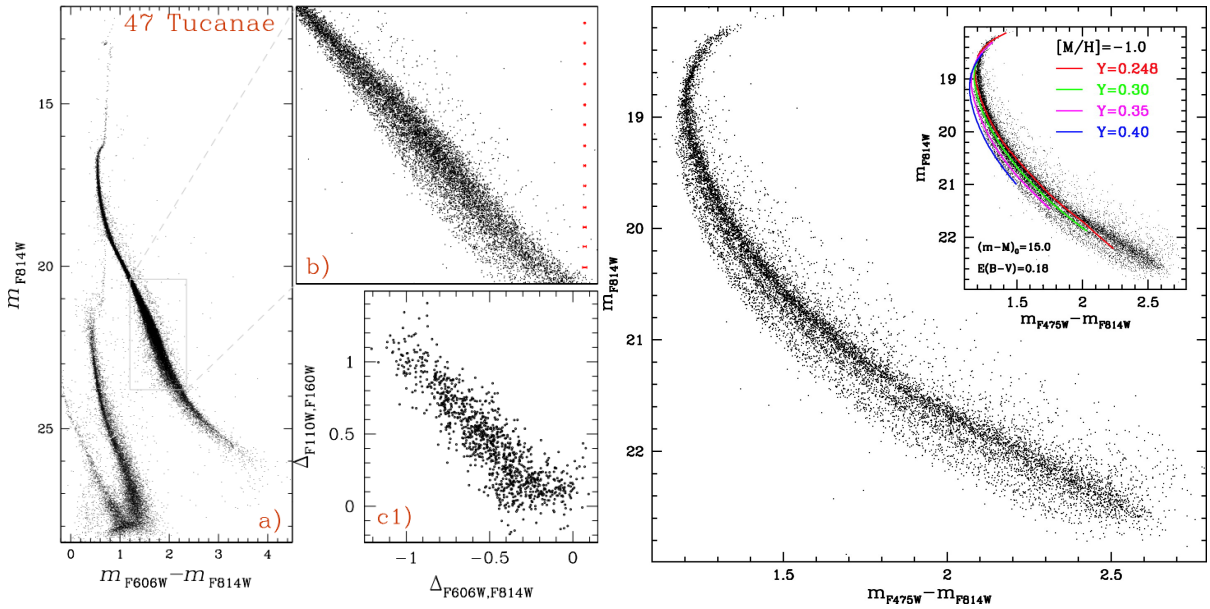

Figure 1. *Left:* The CMD of 47 Tucanae. Subplot b shows the zoomed-in main sequence branch of the cluster. Its spread indicates that the cluster possibly contains multiple stellar populations [2]. *Right:* The CMD of NGC 2808 whose main sequence branch is divided into three branches. The subplot depicts the isochrones of different metallicities present in the cluster, which revealed the cluster's multiple populations [9].

As mentioned in the previous section, the existence of multiple populations in GCs could be explained by the cluster having multiple epochs of star formation. This would entail that the first population forms similarly to stars in an open cluster, as the result of the collapse of a MC. When the first stars have evolved to the asymptotic giant branch, these stars will eject gas that is richer in metals than the MC the cluster originated from. This gas mixes with metal-poor gas already present in the cluster, cools down and forms a second population of metal-richer stars. This process would elongate the currently believed duration of star formation in clusters and can even contain multiple bursts of star formation when also considering the ejecta of supernovae and the second population when it evolves to the asymptotic giant branch as sources of metal-rich gas [10].

Another popular theory proposes that stars within GCs formed around the same time, yet a portion of these stars accreted enriched gas during the pre-main sequence phase. The basis of this theory is that

during the formation of the cluster, gas flows contracted the cluster. Due to an increase in density and consequently stellar collisions, supermassive stars form as long as two-body relaxation does not stop the contraction of the cluster. The powerful, metal-rich winds of these stars mix with metal-poor gas already present in the cluster and are accreted by other stars in the cluster, thereby rejuvenating them [11].

2.2 Our hypothesis

Every theory proposed thus far can either not explain all features of MPs or does not have any observational evidence to support it. Therefore, in this project, we propose a new formation mechanism: during the collision of a GC and a MC, the stars of the cluster accrete mass from the cloud, enriching the stars in the process.

Such a collision is possible in the Milky Way due to the distribution of MCs and the orbits of GCs. MCs are primarily located around the spiral arms of the Galaxy. These arms are constrained to the Galactic Plane [7]. GCs orbit the Galactic Centre on often highly eccentric trajectories with a wide range of inclinations. In their orbits, the clusters cross the Galactic Plane multiple times. Considering their age, we therefore believe that some, if not most, GCs will travel through a MC at least once in their lifetime. To further illustrate this, the left plot of Fig 2 depicts the distance to the Galactic Plane of NGC 2808, which has three distinct main sequence branches, as a function of its distance to the Galactic Centre in the last 500 Myr. The cluster passes through the plane seven times during this period. The right plot of the figure shows the orbit of NGC 2808 in the X-Y plane, with the Milky Way and its spiral arms in the background.

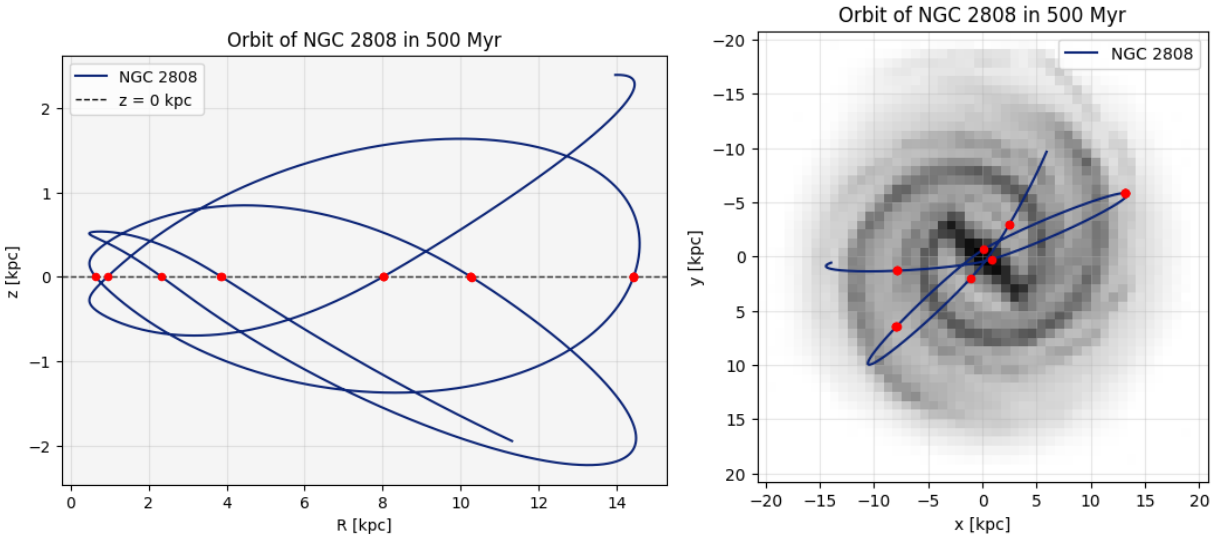

Figure 2. *Left:* The distance to the Galactic Plane as a function of the distance to the Galactic Centre of NGC 2808 in the last 500 Myr. The red dots indicate each instance the cluster travels through the plane. *Right:* The orbit of NGC 2808 in the X-Y plane in the last 500 yr. The dots indicate each instance the cluster travels through the plane. The Milky Way is shown in the background.

Since Galactic GCs have radial velocities between 0.3 and 500 km s^{-1} [12] and MCs typically have a diameter of a few tens of parsecs [7], a GC can traverse MCs within a few kyr to Myr. Slow clusters, with velocities lower than $\approx$ 100 km s^{-1}, are of particular interest for our theory. They are slow enough

to accrete material from the MC as they pass through it. This process creates an enriched layer around the stars that distinguishes them from stars that do not accrete any or enough material, leading to the formation of a second stellar population.

Considering that stars with low metallicities produce less disruptive stellar winds [13], we believe that stars in GCs will not lose a significant amount of the accreted material. If a cluster later travels through another MC with a different metallicity, it can form another population and/or enrich the existing one.

3 Methods

3.1 Simulation Setup

In order to model the problem, we considered the three-dimensional simulation for a single passage of a GC through a spherical MC. The accretion of cloud gas particles onto each star and the consequential stellar mass increase were investigated. No star formation was taken into account for this experiment.

For the scope of a one-semester project, the initial parameter space was reduced to only two variables, namely the cluster's velocity and the number of stars. The velocity is inversely related to the amount of time a star spends inside the cloud, constraining the interaction. The variation in the number of stars contributes to a balance between computational expenses and realistic representations, which will be further discussed in section 3.2. A complete parameter space with regard to this physics configuration is listed in Fig 3.

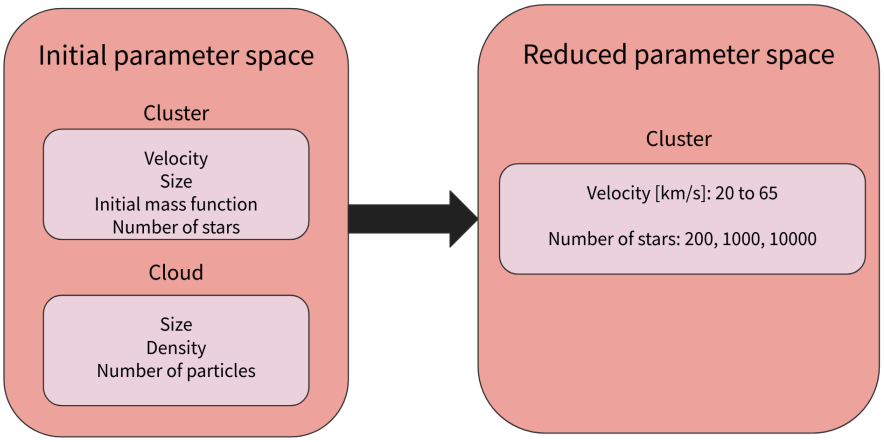

Figure 3. Initial parameter space for this experiment. The left panel shows all possible parameters for our setup, and the right shows the parameters investigated during this project.

The MC was initialized with a 15 pc radius. A constant initial density profile of 23 amu cm^{-3} was assigned, assuming mostly molecular hydrogen. The cloud was evolved hydrodynamically for 2 Myr so the internal structures became apparent. Spontaneous star formation was prevented given that the maximum local density after evolution was only 1.6×10^{-22} g cm^{-3} [14].

For the initial conditions of the GC, a Kroupa initial mass distribution [15] was used to create an ensemble of stars between 0.2 $M_\odot$ and 7 $M_\odot$. The stars were saved in an `AMUSE` particles set and a metallicity

one-tenth of the solar metallicity was given. We then used the stellar evolution simulator SeBa [16] to evolve the cluster to 10 Gyr old, ensuring that every star had the appropriate mass and evolutionary stage for a typical GC. So the most massive stars initiated to be 7 $M_\odot$ are now around 1 $M_\odot$ after stellar evolution. A King model density profile [17] with $w_0 = 3$ was used to revirialize the post-evolution cluster into an equilibrium position with a core radius of 4 pc.

The model started with the center of mass of the cluster and the cloud aligned along the x-axis, with the cloud at the origin and the cluster at -30 pc. During the simulation, the cluster is given a positive initial velocity only in the x direction. The total evolution time for the collision is varied for runs with different velocities in order to make sure that the stars can leave the cloud completely, as shown in Tab 1. Only face-on collisions were considered. Fig 4 presents this encounter progress for a sample run. The masses and positions of the stars were recorded at every time step to account for accretion analysis.

Cluster velocity [kms^{-1}]	20	25	30	35	40	45	50	55	60	65
Total time evolved [Myr]	2.8	2.4	2.2	2.0	1.8	1.7	1.6	1.3	1.0	0.8

Table 1. A summary of all tested cluster velocities and their corresponding evolutionary time.

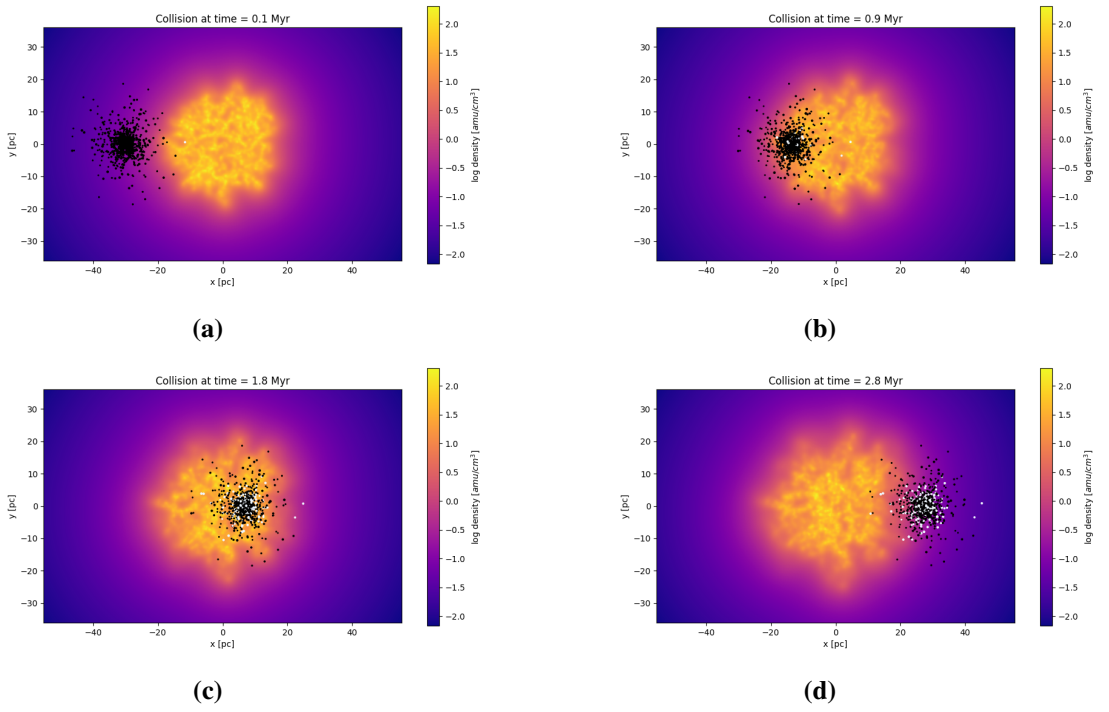

Figure 4. Snapshots of the system as a 200 stars cluster passes through the MC at 20 km s^{-1}. White points represent stars that have accreted at least once on or before the current time step. All star and cloud particle positions are projected onto the X-Y plane.

3.2 Implementation

To account for the mass accretion effect during the evolution, sink particles are created corresponding to the initialized stars. These sink particles are the ones being evolved during our simulation. The gravitational N-body interactions of the stars are integrated using the hierarchical tree code BHTree [18] which provided us with enough accuracy while being fast. For the evolution of the stars during the simulation, SSE [19] was used since it was the only stellar evolution code we found in `AMUSE` that allows for updating stellar masses as it runs. To initialize and evolve the MC, the `AMUSE` integrated smoothed particle hydrodynamics (SPH) code Fi is used [20]. Given that the minimum stellar mass in the cluster is around 0.2 $M_{\odot}$, the number of SPH particles is controlled to prevent the mass of a gas particle from exceeding 0.05 $M_{\odot}$, allowing accretions. A bridge is used to couple the hydrodynamic code Fi with the N-body code BHTree, ensuring that our cloud gas particles are affected by the gravity from the sink particles in the GC. An illustration of this code layout is shown in Fig 5.

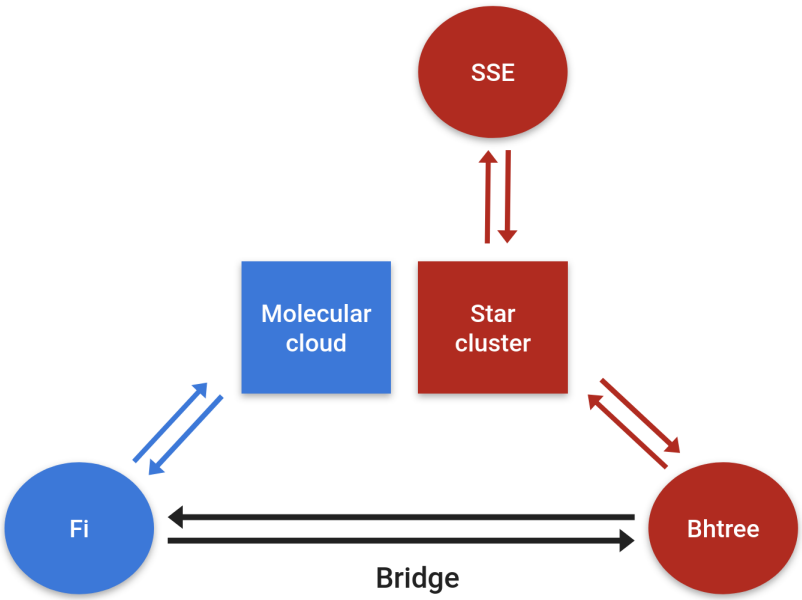

Figure 5. A flowchart connecting the evolution targets and the `AMUSE` modules for different physics processes. `Fi` [20], `SSE` [21], and `Bhtree` [18] correspond to hydrodynamics, stellar evolution, and gravity, respectively. Code coupling is achieved via `AMUSE` channels and a bridge.

The total evolution time of each run differs by the cluster velocity but the integration time step is always set to be 0.1 Myr. At every time step, the stars are first evolved by SSE to model their stellar evolution and monitor for possible mass loss through stellar winds. Such a scenario would greatly affect the local ambient medium and temporarily halt accretion episodes. Then the bridge calls for the gravity and hydrodynamics codes to simulate and update the position of particles. The accretion happens at last for the sink particle stars to update the mass at the end of every time step.

Three layers of accretion criteria were set. First, the sink radius of each particle is calculated to be the Bondi radius [22] of the star

$$R_{Bondi} = \frac{2GM}{c_s^2}, \tag{1}$$

where G is the gravitational constant, M is the mass of the star, and c_s is the sound speed of the medium. Here a typical MC sound speed value of 0.2 km s^{-1} [14] was taken. For the gas particles within R_{Bondi}, the average kinetic energy of the ensemble is compared to the specific binding energy between the star and the gas to determine whether the gas is gravitationally bound to the star. Finally, we calculated the free-fall velocity for a gas to drop onto the surface of the star and found the maximum distance travelled at this velocity within a time step, $R_{ff} = dt \times v_{ff}$. This radius is compared to the real distance between the gas particles and the star. If the free-fall radius R_{ff} is smaller than the real distance, only a fraction of the gas can be accreted, depending on the density distribution within the free-fall radius. For a gas particle that underwent partial accretion, its mass is also updated accordingly.

Most of this package is built and tested on our personal laptops with clusters of 200 stars, much less than the typical number of around 10^5. In order to generate a more realistic representation, the compute resources from the Academic Leiden Interdisciplinary Cluster Environment (ALICE) provided by Leiden University was used to simulate the encounter for a 1000 star cluster and a 10,000 star cluster. Due to the rising cost of computing capabilities, convergence tests with time steps 0.05 Myr and 0.01 Myr, and different initialization random seeds were also produced on ALICE. For testing on personal computers or laptops, an example script for the collision of a GC with 1000 stars and a 20 km s^{-1} velocity is provided.

4 Results

The focus of the project is on stellar rejuvenation through external mass accretion, as described in Sec 1. During a passage of the GC through the MC, we monitor the amount of mass accreted onto the i-th star of the cluster. We do this by representing the cluster's stars with `AMUSE` sink particles, as described in Sec 3.

4.1 Mass Accretion

Fig 6 shows the mass accretion history of all stars that experienced accretion episodes through the entire simulation time. In the current simulation setup, the percentage of stars that underwent such accretion episodes is around $\sim$ 30-45%.

A histogram of the total, relative mass accreted is shown in Fig 7. In this plot, we can see the distribution of accreted mass, with the majority of accreting stars accumulating only a small fraction of their initial mass. This holds even in the case of the lowest collision velocity, shown in Figs 6 & 7, where we expect the most pronounced accretion episodes.

Next, we examined the total mass accretion for different impact velocities. We repeated the simulation for a range of collision velocities between 20 and 65 km s^{-1}. For each different velocity value, we repeated the simulation 19 times, each time changing the random seeds used to initialize the cloud and the cluster. This gave us a set of 19 different values for the total mass accreted, for each velocity value. Finally, the

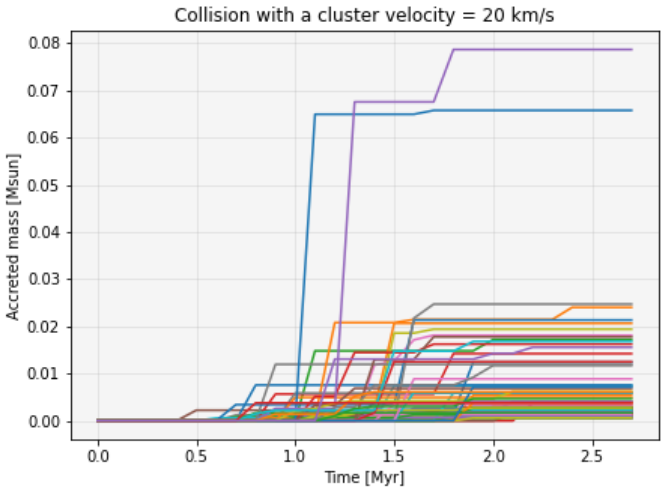

Figure 6. Mass of the accreted material with respect to time for all stars in the cluster that experienced mass accretion episodes. This plot shows the history of mass accretion for a simulation run with 200 stars in the GC and a molecular cloud of R = 15 pc.

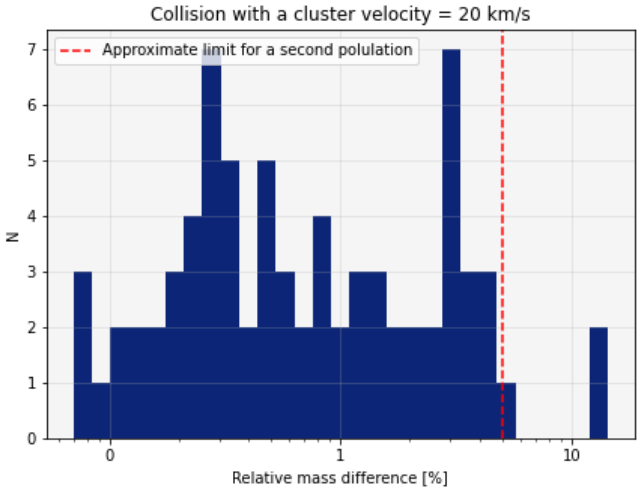

Figure 7. Histogram of the relative mass accreted onto the stars, on semi-log axes. Red, dashed line indicates an approximate boundary for the relative mass needed to show a distinct stellar population on the HR diagram (see section 4.2). This plot shows the history of mass accretion for a simulation run with 200 stars in the GC and a molecular cloud of R = 15 pc.

reported value of the total mass accretion at each velocity is the mean value of the aforementioned set, while its error is quantified as the standard deviation. Fig 8, shows the results of this study.

The size of the MC remained constant through the different simulations described here. This means that the cluster travelled the same distance but, with increasing velocity, the time spent in the cloud is reduced, as it is inversely proportional to the velocity (r = constant = v · t). We expect that the total mass accretion

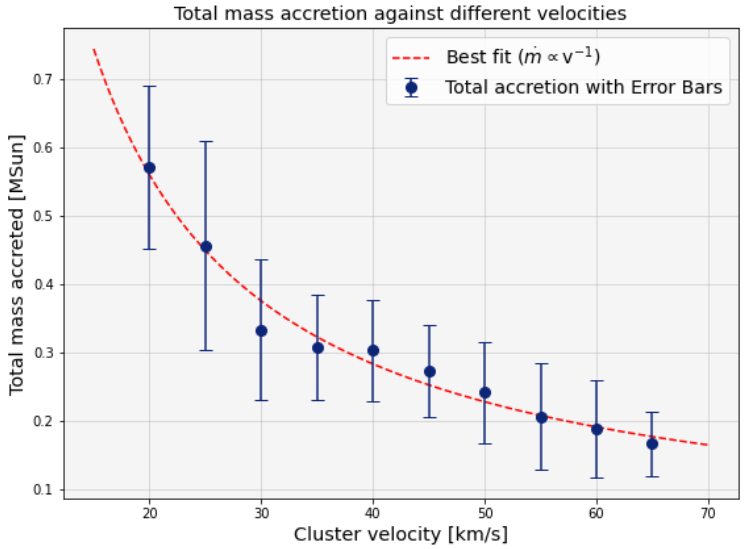

Figure 8. Total accreted mass with respect to different impact velocities. For each velocity value, 19 different simulation runs, with different random seed each, yielded a set of 19 values for the total accreted mass. The mean value of the set is the reported value of total accreted mass and the stadard deviation in the set is the error of the measurement. Red, dashed line shows the best fitted curve under the assumption that the total accreted mass is inversely proportional to velocity. All simulation runs are with 200 stars in the GC and a molecular cloud of R = 15 pc

is proportional to the time the cluster spent within the cloud. Therefore $\dot{m} \propto v^{-1}$. Indeed, if we fit the data with a curve of the form

$$\dot{m} = a \cdot v^{-1} + b \tag{2}$$

the best-fitted curve closely follows the mass accretion trend, as is evident in Fig 8. The coefficients of the best-fitted line are here a = 11.08 and b = 0.01.

4.2 Stellar Metallicities

The smoking gun of multiple stellar populations in clusters is the apparent spread of the main sequence track on the Hertzsprung–Russell diagram. This spread is caused by stars on different stellar isochrones. Stars that follow different isochrones have different spectral behaviour which can be quantified by their metallicity. Stellar metallicity is defined as the mass fraction of all elements heavier than helium

$$Z = 1 - \frac{m_H}{M} - \frac{m_{He}}{M}. \tag{3}$$

Rearranging Eq 3, one can compute the dependence of the mass of hydrogen and helium components on the metallicity and total mass

$$m_H + m_{He} = M(1 - Z). \tag{4}$$

Using Eq 4, we can update the metallicity of the i-th star that has accreted material from a MC of mass $M_{material}$ as

$$Z_{\star,final} = 1 - \frac{M_{\star,initial}(1 - Z_{\star,initial}) + M_{material}(1 - Z_{MC})}{M_{\star,final}}. \quad (5)$$

We have pre-evolved the cluster with a metallicity of Z = 0.002, corresponding to population II. We further assume the molecular cloud to be richer in metals, with a metallicity of Z = 0.02 corresponding to population I. Using Eq 5 and the total mass accreted onto the stars, we can update their metallicities. Fig 9 shows the distribution of the metallicity of the stars that have accreted mass during the passage through the cloud.

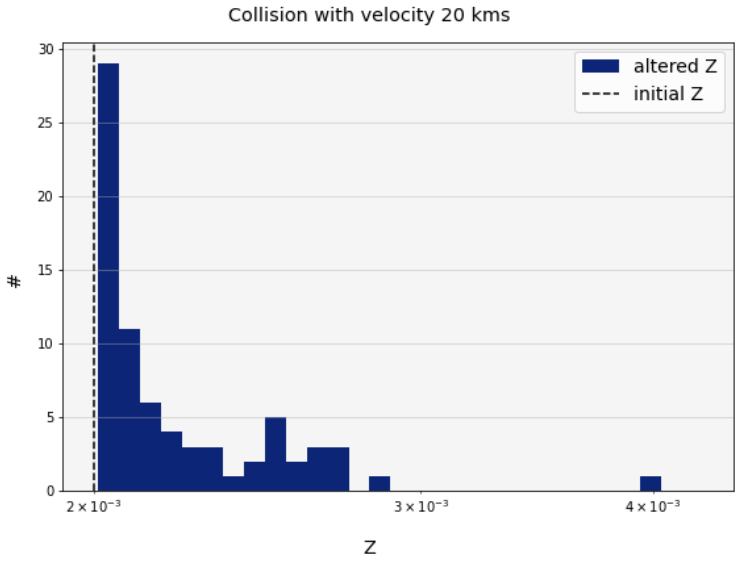

Figure 9. Histogram of the updated metallicity of stars that experienced mass accretion episodes, on semi-log axes. Black, dashed line indicates the initial metallicity of the stars in the cluster, prior to the simulation. This plot shows the history of mass accretion for a simulation run with 200 stars in the GC and a molecular cloud of R = 15 pc.

Eq 5 relates the new metallicity of a star to the total mass that it has accreted. We used it to qualitatively define an approximate boundary for the mass accretion needed to form an observable second stellar population. We did that by setting up a toy simulation of the stellar evolution of two stellar populations with the exact same IMF and number of stars but different metallicities, one fixed at the population II value (Z = 0.002) and the other being the test metallicity. We noticed that the main sequence broadening was detectable once the value of the test metallicity corresponded to a mass accretion of $\sim 5\%$ (see Fig 7). We have to note that this is a back-of-the-envelope calculation and thus should be taken with a grain of salt.

4.3 Hertzsprung–Russell diagram

The increase in metallicity for the stars that accreted material from the cloud, shown in Fig 9, can potentially lead to the aforementioned spread of the main sequence track on the HR diagram. To explore this possibility, after the end of the simulation run, we modelled the stellar evolution of the 200 stars in

the cluster with SeBa code. We used the stars' initial mass as their birth mass and if the i-th star had an updated metallicity at the end of our simulated collision, we used this final value for its evolution. We evolve for $t_{SE} = t_{GCage} + t_{collision}$ and we plot the HR diagram in Fig 10. We see that indeed the position of some stars that accreted mass on the HR diagram is shifted higher than the position of the non-accreting stars.

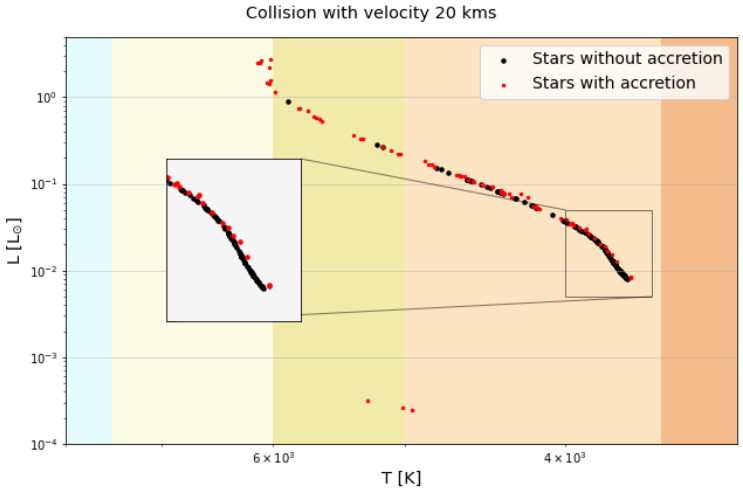

Figure 10. HR diagram of the stars in the cluster after the collision. Red markers indicate stars that have accreted some material from the cloud, while black markers correspond to stars with no accretion episodes. The colored background indicates the Harvard spectral classification scheme for stars on the main sequence branch [23]. From right to left, sandy-brown corresponds to Class M, navajo-white to Class K, khaki to Class G, light-yellow to Class F and light-cyan to Class A. This HR diagram corresponds to a simulation run with 200 stars in the GC and a MC with a radius = 15 pc.

4.3.1 HR diagram of a simulation run with 10,000 stars

Having picked up a slight spread on the main sequence track in the naive case of a star cluster with 200 stars, we decided to model a more realistic scenario, this time with a cluster comprised of 10,000 stars. The rest of the simulation setup remained the same. The computational needs for such an expensive run were met with the usage of ALICE nodes, as described in Sec 3.2. Repeating the same data analysis of the simulation outputs, as before, we plot the HR diagram of the 10,000 stars in Fig 11. This time, the main sequence spread is clearly visible and similar to observational studies of GCs with multiple stellar populations (see [1, 2]). Consequently, this result is the observational signature of the stellar rejuvenation mechanism modelled in our study.

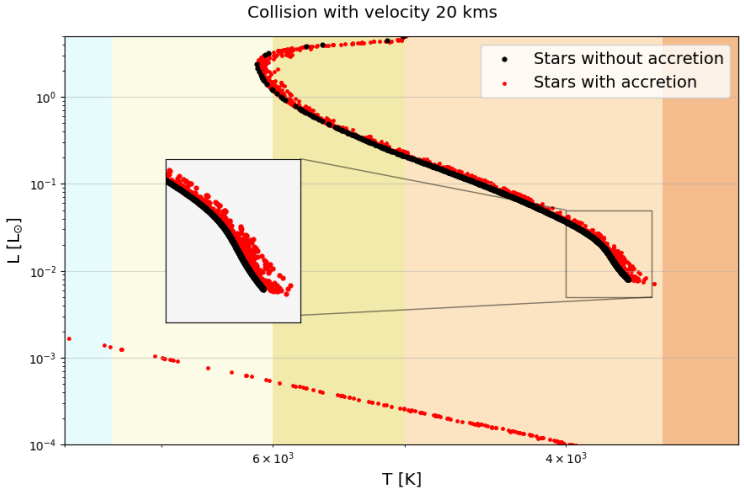

Figure 11. HR diagram of the stars in the cluster after the collision. Red markers indicate stars that have accreted some material from the cloud, while black markers correspond to stars with no accretion episodes. The colored background indicates the Harvard spectral classification scheme for stars on the Main Sequence [23]. From right to left, sandy-brown corresponds to Class M, navajo-white to Class K, khaki to Class G, light-yellow to Class F and light-cyan to Class A. This HR diagram corresponds to a simulation run with 10,000 stars in the GC and a MC with a radius = 15 pc.

5 Discussion

Due to time constraints, our study focused on investigating the impact of a cluster's velocity on the amount of mass accretion following the collision with a MC. A potential future direction could be analyzing how MCs with different densities would impact the mass transfer accordingly. In addition, we were limited in the amount of SPH particles in the cloud due to the computational expenses. With more SPH particles, the simulated cloud would be more realistic. To validate the dispersion of stars along the main sequence branch, as depicted in Fig 11, the logical next step involves conducting a repeat simulation of the 10,000-star model within a denser cloud and more SPH particles.

As illustrated previously in Sec 2.2, GCs pass through the Galactic Plane multiple times during their lifetime. Therefore, future experiments should consider multiple collisions occurring over extended time spans. Accounting for stellar evolution between collisions and examining the resulting mass loss are crucial, especially given the 100 Myr time scales involved in this scenario.

Another intriguing avenue for future research involves incorporating star formation processes within the cloud. Our current study only investigated a cloud without spontaneous star formation, a condition not so representative of the dense MCs within the central Galactic Plane. Exploring clouds susceptible to star formation could allow future scientists to understand whether collisions between GCs and such clouds would impact the rate of star formation. Furthermore, this investigation could shed light on the possibility of stars being stripped away from the cloud, potentially leading to the emergence of a secondary population of stars in the GC, explaining the broadened main sequence branch that has been observed.

6 Conclusion

In our study, we put forward a hypothesis regarding the formation of a second, younger, stellar population within a GC. This formation channel is solely founded on the stellar rejuvenation of some stars through external mass accretion. The site in which we hypothesised such an accretion to take place, is the inner parts of a metal-richer MC. An encounter of a GC with an MC is highly probable for GCs with favourable eccentricities and inclinations and can occur during their crossing of the Galactic mid-plane, where the MCs are settled, as discussed in Sec 2.2.

To study the plausibility of such a scenario, we modelled a collision between a GC and an MC using `AMUSE`. The complexity of such an encounter was reduced to a simple scenario of a face-on collision, with varying impact velocities, due to time constraints. Furthermore, the MC was restricted to an unperturbed MC in hydrostatic equilibrium, thus no star-forming regions were taken into consideration. Moreover, while the stars were evolved with the `SSE` stellar code during the simulation, only their mass was altered in cases of accretion and not their metallicity. A parallel update of their metal content could lead to stellar winds, while in our naive case, we do not observe any wind. Finally, the GC was modelled with the `BHTree` N-body solver, the MC was simulated with the `Fi` SPH code and the two codes were coupled bidirectionally with the `bridge` class of `AMUSE`.

Even in this simple case studied here, some important results arise and they are summarised below;

1. External mass accretion onto stars of GCs, after an impact with an MC, is, in principle, a viable scenario for the formation of a second stellar population in GCs.
2. The total mass accreted by a GC in such a collision with an unperturbed MC, is inversely proportional to the impact velocity.
3. Mass accretion from a metal-richer MC leads to stellar rejuvenation. The rejuvenation modelled in this study is in agreement with the observational signature of multiple stellar populations in GCs. For that reason, studies on the origin of multiple stellar populations in GCs should take into consideration the external mass accretion scenario.

References

[1] N. Bastian and C. Lardo, "Multiple stellar populations in globular clusters," *Annual review of Astronomy and Astrophysics*, vol. 56, pp. 83–136, 2018.

[2] A. P. Milone and A. F. Marino, "Multiple Populations in Star Clusters," *Universe*, vol. 8, p. 359, June 2022.

[3] S. F. Portegies Zwart, S. McMillan, S. Harfst, D. Groen, M. Fujii, B. Ó. Nualláin, E. Glebbeek, D. Heggie, J. Lombardi, P. Hut, *et al.*, "A multiphysics and multiscale software environment for modeling astrophysical systems," *New Astronomy*, vol. 14, no. 4, pp. 369–378, 2009.

[4] F. Pelupessy, A. Van Elteren, N. De Vries, S. McMillan, N. Drost, and S. F. Portegies Zwart, "The astrophysical multipurpose software environment," *Astronomy & Astrophysics*, vol. 557, p. A84, 2013.

[5] S. F. Portegies Zwart, S. L. McMillan, A. van Elteren, F. I. Pelupessy, and N. de Vries, "Multi-physics simulations using a hierarchical interchangeable software interface," *Computer Physics Communications*, vol. 184, no. 3, pp. 456–468, 2013.

[6] S. F. Portegies Zwart and S. McMillan, *Astrophysical Recipes: the art of AMUSE*. IoP Publishing, 2018.

[7] D. Maoz, *Astrophysics in a Nutshell*, vol. 16. Princeton university press, 2016.

[8] S. Cassisi and M. Salaris, "Multiple populations in massive star clusters under the magnifying glass of photometry: Theory and tools," *The Astronomy and Astrophysics Review*, vol. 28, no. 1, p. 5, 2020.

[9] G. Piotto, L. Bedin, J. Anderson, I. King, S. Cassisi, A. Milone, S. Villanova, A. Pietrinferni, and A. Renzini, "A triple main sequence in the globular cluster ngc 2808," *The Astrophysical Journal*, vol. 661, no. 1, p. L53, 2007.

[10] A. D'Ercole, E. Vesperini, F. D'Antona, S. L. McMillan, and S. Recchi, "Formation and dynamical evolution of multiple stellar generations in globular clusters," *Monthly Notices of the Royal Astronomical Society*, vol. 391, no. 2, pp. 825–843, 2008.

[11] M. Gieles, C. Charbonnel, M. G. Krause, V. Hénault-Brunet, O. Agertz, H. J. Lamers, N. Bastian, A. Gualandris, A. Zocchi, and J. A. Petts, "Concurrent formation of supermassive stars and globular clusters: implications for early self-enrichment," *Monthly Notices of the Royal Astronomical Society*, vol. 478, no. 2, pp. 2461–2479, 2018.

[12] H. Baumgardt, A. Sollima, M. Hilker, A. Bellini, E. Vasiliev, V. Henault-Brunet, and N. Dickson, "Fundamental parameters of galactic globular clusters," database, The University of Queensland, Australia, 2023.

[13] R. P. Kudritzki, "Line-driven winds, ionizing fluxes, and ultraviolet spectra of hot stars at extremely low metallicity. i. very massive o stars," *The Astrophysical Journal*, vol. 577, no. 1, p. 389, 2002.

[14] M. R. Krumholz, E. Telles, R. Dupke, and D. Lazzaro, "Star formation in molecular clouds," in *AIP Conference Proceedings*, AIP, 2011.

[15] P. Kroupa, "On the variation of the initial mass function," , vol. 322, pp. 231–246, Apr. 2001.

[16] S. F. Portegies Zwart and F. Verbunt, "SeBa: Stellar and binary evolution." Astrophysics Source Code Library, record ascl:1201.003, Jan. 2012.

[17] I. R. King, "The structure of star clusters. III. Some simple dynamical models," , vol. 71, p. 64, Feb. 1966.

[18] J. Barnes and P. Hut, "A hierarchical O(N log N) force-calculation algorithm," , vol. 324, pp. 446–449, Dec. 1986.

[19] J. R. Hurley, O. R. Pols, and C. A. Tout, "Comprehensive analytic formulae for stellar evolution as a function of mass and metallicity," *Monthly Notices of the Royal Astronomical Society*, vol. 315, p. 543–569, July 2000.

[20] L. Hernquist and N. Katz, "TREESPH: A Unification of SPH with the Hierarchical Tree Method," , vol. 70, p. 419, June 1989.

[21] J. R. Hurley, O. R. Pols, and C. A. Tout, "SSE: Single Star Evolution." Astrophysics Source Code Library, record ascl:1303.015, Mar. 2013.

[22] H. Bondi, "On spherically symmetrical accretion," , vol. 112, p. 195, Jan. 1952.

[23] A. J. Cannon and E. C. Pickering, "Spectra of bright southern stars photographed with the 13-inch Boyden telescope as part of the Henry Draper Memorial," *Annals of Harvard College Observatory*, vol. 28, pp. 129–P.6, Jan. 1901.